

Review

The Development of Bispecific Hexavalent Antibodies as a Novel Class of DOCK-AND-LOCK™ (DNL™) Complexes

Chien-Hsing Chang^{1,2,*}, Edmund A. Rossi^{1,2}, Yang Wang¹, Thomas M. Cardillo¹ and David M. Goldenberg^{1,2,3,*}

¹ Immunomedics, Inc., Morris Plains, NJ 07950, USA

² IBC Pharmaceutical, Inc., Morris Plains, NJ 07950, USA

³ Garden State Cancer Center, Center of Immunology and Molecular Medicine, Morris Plains, NJ 07950, USA

* Authors to whom correspondence should be addressed; E-Mails: kchang@immunomedics.com (C.-H.C.); dmg.gscancer@att.net (D.M.G.).

Received: 1 March 2013; in revised form: 9 May 2013 / Accepted: 13 May 2013 /

Published: 23 May 2013

Abstract: The DOCK-AND-LOCK™ (DNL™) method provides a modular approach to develop multivalent, multifunctional complexes of defined structures, of which bispecific hexavalent antibodies (bsHexAbs) are prominent examples with potential applications in targeted therapy for malignant, autoimmune, and infectious diseases. Currently, bsHexAbs are constructed by derivatizing a divalent IgG, at the carboxyl termini of either the heavy chain (the C_H3-format) or the light chain (the C_K-format), to contain two stabilized dimers of Fab having a different specificity from the IgG. In this review, we briefly outline the features of the DNL™ method and describe key aspects of bsHexAbs examined with diverse preclinical studies, which include binding affinity to target cells, induction of signaling pathways, effector functions, serum stability, pharmacokinetics, and antitumor activity in human tumor xenograft models. Our findings favor the selection of the C_K- over the C_H3-format for further exploration of bsHexAbs in clinical trials.

Keywords: DNL™; bispecific; hexavalent; conjugation; site-specific; antibodies; cancer

1. Introduction

With more than 30 antibody-based products now commercialized, and an additional 28 in advanced clinical trials for various indications [1], the prospect of monoclonal antibodies (mAbs) as next-generation therapeutics has been realized. Since the efficacy of mAbs often can be enhanced when combined with other antibodies targeting different antigens [2–8], or distinct epitopes of the same antigen [9,10], parallel efforts to explore the potential of combination therapy with dissimilar antibodies are being explored. In principle, combination therapy involving two unlike antibodies could be accomplished more cost-effectively with a cognate dual-targeting bispecific antibody (bsAb). Accordingly, there has been an emergence of new bsAbs that differ in design, structure, valency, and specificity [11,12].

The basic format of a divalent bsAb comprises two half-molecules of IgG, each with a different antigen-binding specificity. Although such bsAbs may form in nature as a result of dynamic Fab-arm exchange involving two different IgG4 molecules [13–15], they were at first generated for potential applications either from quadromas [16,17] via fusing two hybridomas, or through chemical crosslinking of IgG [18] or Fab' [19,20]. Subsequent efforts were directed primarily toward recombinant engineering of Fc-lacking [21,22], as well as Fc-containing [23], bsAbs, with a more recent interest in the construction of tetravalent, IgG-like bsAbs [24] that vary in design, structure and antigen-binding constituents [25–31].

We have advanced an alternative approach of constructing bsAbs using the DOCK-AND-LOCK™ (DNL™) method [32–35], which enables the site-specific self-assembly of two modular components only with each other, resulting, after combining under mild redox conditions, in a covalent structure of defined composition with retained bioactivity. The initial proof-of concept was provided by linking a stabilized dimer of Fab specific for one antigen to a monomeric Fab with specificity for a different antigen to generate a bispecific trivalent antibody composed of three stably-tethered Fab-arms [32]. Since then, we have applied the DNL method to develop bispecific hexavalent antibodies (bsHexAbs) by derivatizing a divalent IgG, at the carboxyl termini of either the heavy chain (the C_{H3}-format), or the light chain (the C_κ-format), to contain two stabilized dimers of Fab with a different specificity from the IgG [36–40]. In this review, we present archetype examples of bsHexAbs and discuss the notable advantages of the C_κ-format over the C_{H3}-format as revealed by preclinical results.

2. The DNL™ Method

The DNL™ (henceforth, DNL) method is based on the specific protein/protein interactions occurring in nature between the regulatory (R) subunits of cAMP-dependent protein kinase A (PKA) and the anchoring domain (AD) of an interactive A-kinase anchoring protein (AKAP) [41,42]. There are two types of R subunits (RI and RII) found in PKA and each has α and β isoforms. The R subunits contain a dimerization domain in the first 44 amino-terminal residues and have been isolated only as stable dimers [43]. The AD of AKAPs for PKA is an amphipathic helix of 14–18 residues [44], which binds only to dimeric R subunits. For human RII α , the AD binds to a hydrophobic surface formed by the 23 amino-terminal residues [45]. Thus, the dimerization domain and AKAP binding domain of human RII α are both located within the same N-terminal 44 amino acid sequence [43,46], and are referred to as the dimerization and docking domain (DDD).

While pursuing a trivalent bispecific antibody-based agent best suitable for pretargeting applications [47–49], we recognized the prospect of exploring a DDD and its cognate AD as an attractive pair of linkers, and envisioned the feasibility of specifically docking a module containing the DDD of human RII α , referred to as DDD1, with a module containing *AKAP-IS* [50], a synthetic peptide optimized for RII-selective binding with a reported K_D of 4×10^{-10} M, referred to as AD1, to form a noncovalent complex. This would be locked into a covalently-tethered structure to improve *in vivo* stability by introducing cysteine residues into DDD1 and AD1, resulting in DDD2 and AD2, respectively, to facilitate the formation of disulfide bonds. The amino acid sequences of DDD1, DDD2, AD1 and AD2, as well as a schematic of a basic DNL complex, are shown in Figure 1.

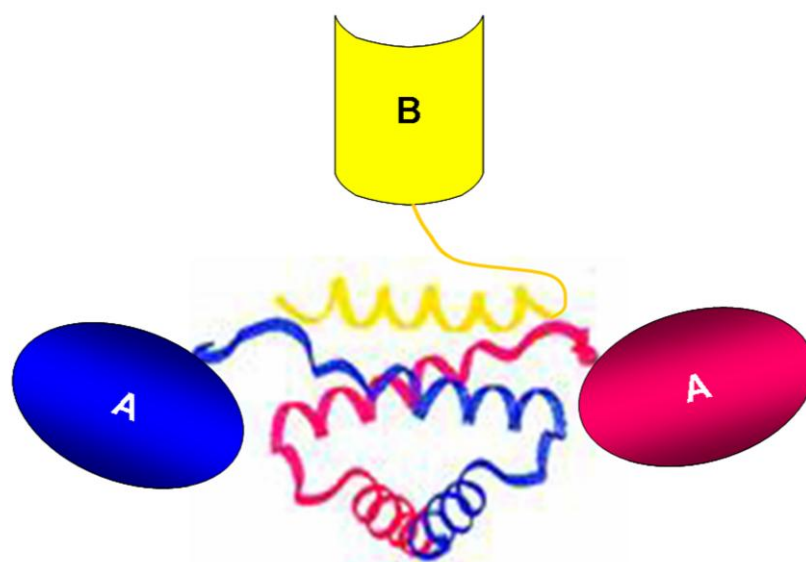
Figure 1. Amino acid sequences (AD1, AD2, DDD1, and DDD2) and a schematic of a basic DNL complex comprising a dimer of A-DDD2 linked to a monomer of B-AD2.

AD1: QIEYLAKQIVDNAIQQA

AD2: CGQIEYLAKQIVDNAIQQAGC

DDD1: HIQIPPGLTELLQGYTVEVLRQQPPDLVEFAVEYFTRLREARA

DDD2: CGHIQIPPGLTELLQGYTVEVLRQQPPDLVEFAVEYFTRLREARA



Besides the unique feature that a module derivatized with the DDD is always presented in two copies, there are additional merits of the DNL method, as summarized below.

DNL is modular. Each DDD- or AD-containing module can be produced independently, stored separately “on shelf,” and combined “on demand.” In principle, any DDD module can be paired with any AD module, and there is essentially no limit on the types of precursors that can be converted into a DDD- or AD-module, so long as the resulting modules do not interfere with the dimerization of DDD or the binding of DDD to AD. In addition to the DDD sequence of human RII α , other DDD sequences may be selected from human RII α , human RII β , or human RII β , and the selected DDD sequence will be matched with a highly interactive AD sequence, which can be deduced from the literature [51] or determined experimentally.

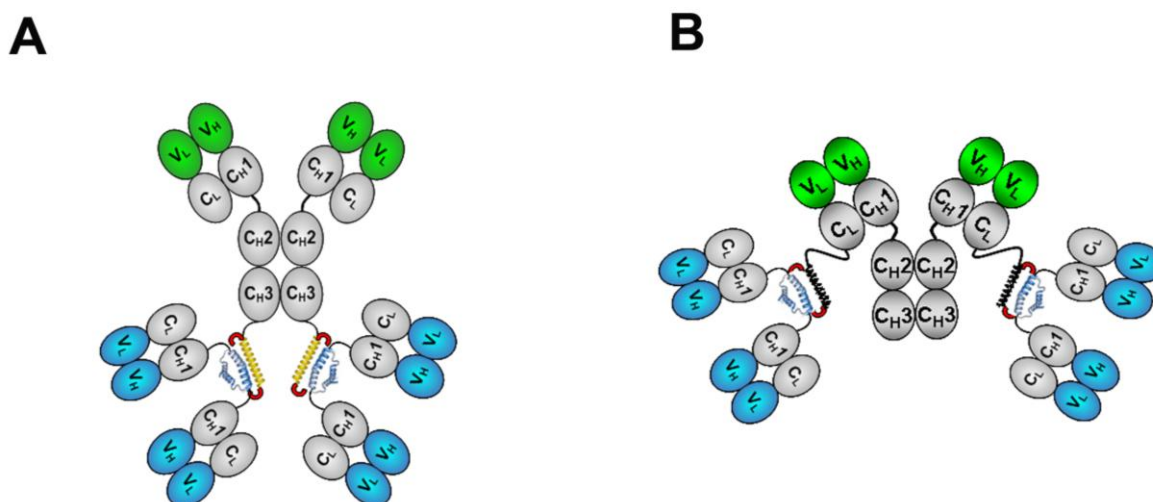
DNL is versatile. The modular nature of the DNL method also makes it versatile, since these modules can be made recombinantly or chemically. A recombinant module may be produced in mammalian or microbial systems, and may derive from antibodies or antibody fragments, cytokines (as shown for interferon- α 2b [52]), enzymes, carrier proteins (such as human serum albumin and human transferrin), or a variety of natural or artificial non-antibody binding or scaffold proteins [53–56]. Although each recombinant module would usually be produced in a separate expression system, we have engineered certain pairs of DDD- and AD-modules for expression in the same host cell without affecting the formation of the DNL complexes. Furthermore, DDD or AD can be coupled to the amino-terminal or carboxyl-terminal end or even positioned internally within the fusion protein, preferably with a spacer containing an appropriate length and composition of amino-acid residues, provided that the binding activity of the DDD or AD and the desired activity of the polypeptide fusion partners are not compromised.

Modules may also be made synthetically, as demonstrated with linking AD2 to either polyethylene glycol or peptides [57], and depending on the intended applications, it should be feasible to develop chemistries for preparing modules that contain peptide mimetics, oligo- or poly-nucleotides, small interfering RNA, chelators with or without radioactive or non-radioactive metals, drugs, dyes, oligosaccharides, natural or synthetic polymeric substances, nanoparticles, dendrimers, fluorescent molecules, or quantum dots.

DNL manufacture is relatively trouble-free and results in quantitative yields of a homogeneous product with a defined composition and retained bioactivities. We have refined the production of the DNL complex into a one-pot reaction followed with three simple steps to recover the product from the starting materials: (i) combine DDD- and AD-modules in stoichiometric amounts; (ii) add redox agents to facilitate the self-assembly of the DNL complex; and (iii) purify by an appropriate affinity chromatography. The spontaneous binding between the DDD and AD modules as well as their site-specific conjugation effects nearly 100% conversion of each into the desired DNL product and assures that the full activity of each module is preserved, the molecular size is homogeneous, the composition is defined, and *in vivo* integrity is largely sustained.

3. The C_H3-format of bsHexAbs

One established application of the DNL method is the generation of the C_H3-format of hexavalent antibodies (HexAbs), all of which comprise a pair of Fab-DDD2 dimers linked to a full IgG at the carboxyl termini of the two heavy chains, thus having six Fab-arms and a common Fc domain, as illustrated Figure 2A. To identify these HexAbs, we assign each of them a code of X-(Y)-(Y), where X and Y are specific designations given to differentiate the antibodies, with the Fab distinguished from the IgG by enclosing its designation in a parenthesis. The present notation is applicable to denote HexAbs that are either bispecific [36–38] or monospecific [58]. As an example, 20-(22)-(22), defines the bsHexAb comprising a divalent anti-CD20 humanized IgG (veltuzumab or hA20) and a pair of dimeric anti-CD22 humanized Fab's (epratuzumab or hLL2). Likewise, 22-(20)-(20) specifies the bsHexAb comprising a divalent hLL2 IgG and a pair of dimeric hA20 Fab's, whereas 20-(20)-(20) describes the monospecific HexAb comprising a divalent hA20 IgG and a pair of dimeric hA20 Fab's. The designation of each antibody used in the construction of bsHexAbs is provided in Table 1.

Figure 2. Schematics of a C_{H3}-based HexAb (A) and a C_K-based HexAb (B).**Table 1.** Designations of antibodies used in the construction of bsHexAbs.

Antigen	Antibody		
	Trivial name	USAN	Designation
CD19	hA19	-	19
CD20	hA20	Veltuzumab	20
CD22	hLL2	Epratuzumab	22
CD74	hLL1	Milatumzumab	74
CEACAM5	hMN-14	Labetuzumab	14
CEACAM6	hMN-15	-	15
HLA-DR	hL243	-	C2
IGF-1R	hR1	-	1R
Trop-2	hRS7	-	E1
Indium-DTPA	h734	-	734

3.1. Generation and Biochemical Analysis

To date, we have made a variety of bsHexAbs in the C_{H3}-format (Table 2) by combining, under mild redox conditions, a C_{H3}-AD2-IgG module with a C_{H1}-DDD2-Fab module, followed by purification with Protein A affinity chromatography. The individual modules used to assemble these HexAbs were produced in mammalian cell cultures and purified by either Protein A (to obtain C_{H3}-AD2-IgG) or *kappa*-select (to obtain C_{H1}-DDD2-Fab). The ensuing DNL reaction typically proceeded uneventfully, resulting in each final conjugate shown by SE-HPLC to consist of a major peak of the expected molecular size (~365 kDa), by SDS-PAGE to be of high purity, and by dynamic light scattering to have an averaged particle diameter of 15.83 nm, about 5 nm larger than an intact IgG [59].

Table 2. Codes, modules, and targets of selected C_H3-based HexAbs.

Code	Alternative name	AD-module		DDD-module	
		Design	Target	Design	Target
20-(22)-(22)	20-22	C _H 3-AD2-IgG-hA20	CD20	C _H 1-DDD2-Fab-hLL2	CD22
22-(20)-(20)	22-20	C _H 3-AD2-IgG-hLL2	CD22	C _H 1-DDD2-Fab-hA20	CD20
20-(74)-(74)	-	C _H 3-AD2-IgG-hA20	CD20	C _H 1-DDD2-Fab-hLL1	CD74
74-(20)-(20)	-	C _H 3-AD2-IgG-hLL1	CD74	C _H 1-DDD2-Fab-hA20	CD20
20-(14)-(14)	20-14	C _H 3-AD2-IgG-hA20	CD20	C _H 1-DDD2-Fab-hMN-14	CEACAM5
22-(14)-(14)	22-14	C _H 3-AD2-IgG-hLL2	CD22	C _H 1-DDD2-Fab-hMN-14	CEACAM5
734-(20)-(20)	734-20	C _H 3-AD2-IgG-h734	Indium-DTPA	C _H 1-DDD2-Fab-hA20	CD20
E1-(1R)-(1R)	-	C _H 3-AD2-IgG-hRS7	Trop-2	C _H 1-DDD2-Fab-hR1	IGF-1R
1R-(E1)-(E1)	-	C _H 3-AD2-IgG-hR1	IGF-1R	C _H 1-DDD2-Fab-hRS7	Trop-2
1R-(15)-(15)	-	C _H 3-AD2-IgG-hR1	IGF-1R	C _H 1-DDD2-Fab-hMN-15	CEACAM6
74-(1R)-(1R)	-	C _H 3-AD2-IgG-hLL1	CD74	C _H 1-DDD2-Fab-hR1	IGF-1R
20-(20)-(20)	Hex-hA20	C _H 3-AD2-IgG-hA20	CD20	C _H 1-DDD2-Fab-hA20	CD20
22-(22)-(22)	Hex-hLL2	C _H 3-AD2-IgG-hLL2	CD22	C _H 1-DDD2-Fab-hLL2	CD22
1R-(1R)-(1R)	Hex-hR1	C _H 3-AD2-IgG-hR1	IGF-1R	C _H 1-DDD2-Fab-hR1	IGF-1R

3.2. Functional Characterizations Based on in Vitro Studies

3.2.1. bsHexAbs that Target CD20 and CD22

With 22-(20)-(20), 20-(22)-(22), and 20-(20)-(20) on hand, we first evaluated the effect of increased valency on binding avidity [36]. Using an anti-idiotypic antibody to veltuzumab as the surrogate antigen, we determined by competition ELISA the binding avidity of the hexavalent 20-(20)-(20) to be 1.4 nM, compared to 2.2 nM and 4.8 nM of the tetravalent 22-(20)-(20) and the divalent 20-(22)-(22), respectively. Similarly, with an anti-idiotypic antibody to epratuzumab as the surrogate antigen, we showed the hexavalent 22-(22)-(22) to display the highest binding avidity (0.30 nM), compared to 0.43 nM and 0.66 nM of the tetravalent 20-(22)-(22) and the divalent 22-(20)-(20), respectively. Furthermore, 20-(22)-(22) and 22-(20)-(20) displayed nearly the same binding avidity as veltuzumab (4.8 vs. 4.9 nM) and epratuzumab (0.66 vs. 0.81 nM), respectively. These results indicate that each Fab-arm in a HexAb retains its binding activity, and the avidity of a divalent IgG can be conveniently enhanced by increasing the valency with the DNL method. Because the enhanced binding avidity of a HexAb due to multiple valencies should slow its dissociation from the surface of bound cells, we also compared the off-rates among veltuzumab, 20-(22)-(22), 22-(20)-(20), and 20-(20)-(20), as measured by flow cytometry using Raji Burkitt lymphoma cells as the CD20/CD22 target, and found them to be 145, 152, 268, and 322 min, respectively [36]. The difference between the hexavalent 20-(20)-(20) and the tetravalent 22-(20)-(20) was statistically significant ($P = 0.0042$), as was the difference between the tetravalent 22-(20)-(20) and the divalent veltuzumab ($P < 0.0001$). However, the difference between 20-(22)-(22) and veltuzumab was not significant ($P = 0.3810$). Thus, the relative off-rates appear to correlate well with the number of CD20-binding arms, but not the number of CD22-binding arms, which may be due to the 10-fold higher expression of CD20 than CD22 in Raji cells.

We then demonstrated the bispecificity of 20-(22)-(22) and 22-(20)-(20) by performing cell-binding analyses with flow cytometry in which Raji cells were pre-incubated with excess C_H1-DDD2-Fab-hA20, C_H1-DDD2-Fab-hLL2, or both, to block CD20, CD22, and CD20/CD22 binding, respectively [36]. Subsequently, cells were stained with a saturating amount of PE (phycoerythrin)-conjugated 22-(20)-(20), 20-(22)-(22), veltuzumab, or epratuzumab, and the resulting fluorescence intensity was measured and compared to that of unblocked control. Without blocking, the MFI (median fluorescence intensity) of cells stained with veltuzumab was approximately 10-fold higher than that observed with epratuzumab, indicating that CD20 is expressed at a considerably higher level than CD22 on Raji cells. Whereas C_H1-DDD2-Fab-hA20, C_H1-DDD2-Fab-hLL2, and the combination completely inhibited veltuzumab, epratuzumab, and all PE-labeled antibodies, respectively, either DDD2-Fab module alone could only partially block 20-(22)-(22) or 22-(20)-(20) from binding to Raji cells, indicating that 20-(22)-(22) and 22-(20)-(20) can bind to both CD20 and CD22 on the target.

We also investigated the extent of internalization of 20-(22)-(22) and 22-(20)-(20) into Raji cells by flow cytometry and made an intriguing observation [36]. Live cells were incubated with PE-conjugated antibodies at 37 °C for 1 h before trypsin digestion to remove non-internalized antibodies. The MFI of cells stained with PE-veltuzumab and PE-22-(20)-(20) was reduced by 90% and 85%, respectively, indicating that 22-(20)-(20) behaves like veltuzumab with a slow internalization rate. On the other hand, we found approximately 50% of the 20-(22)-(22) internalized, similar to the results obtained for epratuzumab. Thus, the internalization property of a bsAb composed of a rapid internalizing antibody, such as epratuzumab, and a slowly or non-internalizing antibody, such as veltuzumab, appears to depend on the relative valency of the two antibodies with different internalization characteristics.

Using a cell counting assay, we further found that 22-(20)-(20) and 20-(22)-(22) effectively inhibited the growth of three Burkitt lymphoma cell lines, Ramos, Raji and Daudi, at 15 nM or lower, whereas under the same conditions, epratuzumab alone was ineffective and veltuzumab alone or in combination with epratuzumab was less effective [36]. Based on the EC₅₀ values determined from dose-response curves, 22-(20)-(20) was more potent than 20-(22)-(22) in the three lymphoma cell lines examined, and the observed direct toxicity was not appreciably affected for either 22-(20)-(20) or 20-(22)-(22) upon the addition of a crosslinking anti-human Fc antibody which, however, markedly increased the inhibitory activity of veltuzumab, but not epratuzumab, alone.

To assess only the effects of divalent, tetravalent, and no binding to CD20 on inhibiting the proliferation of Ramos cells by the MTS assay, we employed the HexAbs of 20-(14)-(14), 734-(20)-(20), and 22-(22)-(22), having two, four, and none of the Fabs of veltuzumab, respectively. As indicated in Table 2, 20-(14)-(14) comprises two Fabs of veltuzumab and four Fabs of labetuzumab (anti-CEACAM5), 734-(20)-(20) comprises two Fabs of 734 (anti-indium-DTPA), and four Fabs of veltuzumab, and 22-(22)-(22) comprises 6 Fabs of epratuzumab with no Fab of veltuzumab. Our finding [36] that the effect of 20-(14)-(14) was similar to that of veltuzumab suggests that the formation of a heterocomplex of CD20 and CD22 on the cell surface is essential for the direct toxicity of 20-(22)-(22). We also confirmed the capability of a tetravalent CD20-binding molecule, such as 734-(20)-(20), to display direct toxicity, and observed no statistical difference between the dose-response curves obtained for 734-(20)-(20) and 22-(20)-(20). On the other hand, the monospecific 22-(22)-(22), which targets only CD22, not CD20, showed no direct toxicity against NHL cell lines *in vitro*, despite its hexavalency. Direct toxicity of 20-(20)-(20), 20-(22)-(22), and 22-(20)-(20) was also evaluated on eight chronic

lymphocytic leukemia (CLL) patient specimens, which varied in their CD20 expression. The three specimens expressing moderate to high CD20 showed 30 to 60% inhibition by the three CD20-targeting HexAbs, while no significant inhibition was observed in the other five specimens with low CD20 expression. It is noted that neither rituximab nor veltuzumab, alone or with hypercrosslinking, produced measurable inhibition in these CLL samples.

We have previously established [60] that veltuzumab, but not epratuzumab, exhibited potent complement-dependent cytotoxicity (CDC), as well as antibody-dependent cellular cytotoxicity (ADCC). Although C_H3-AD2-IgG-hA20, but not C_H3-AD2-IgG-hLL2, induced CDC, as would be expected, the addition of four Fab-components to C_H3-AD2-IgG-hA20, as exemplified by 20-(20)-(20), 20-(22)-(22), and 20-(14)-(14), abolished CDC, and likewise, by 22-(20)-(20). Nevertheless, we could show that 20-(22)-(22), 20-(14)-(14) and 20-(20)-(20) preserved the potent ADCC of veltuzumab; 734-(20)-(20) and 22-(20)-(20) had similar ADCC, either of which was statistically higher ($P = 0.004$) than epratuzumab. These findings support the notion that ADCC is governed primarily by ligation to CD20, and HexAbs based on veltuzumab mediate ADCC more efficiently.

Finally, we have explored the signaling pathways involved in evoking direct toxicity of 20-(20)-(20), 22-(20)-(20), and 20-(22)-(22) in Daudi cells [37], and compared the results with cells treated with anti-IgM antibodies, or with veltuzumab or rituximab in the presence of a crosslinking antibody. Collectively, our findings indicate that the potent direct toxicity of the three CD20-targeting HexAbs is due to their multivalent binding ability, which lowers the threshold for modifying multiple signaling pathways, resulting in a new distribution of pro- and anti-apoptotic proteins that promotes growth arrest, apoptosis, and eventually cell death. Specifically, we showed the following. (i) The signaling events triggered by 20-(20)-(20), 22-(20)-(20), or 20-(22)-(22) were quantitatively and qualitatively similar in Daudi cells, but distinct from those induced by anti-IgM; (ii) Although ligation of CD22 by epratuzumab failed to induce appreciable changes in the basal expression of a variety of signaling molecules examined, ligation of CD20 by veltuzumab or rituximab incurred the signaling events associated with the ERK and NF- κ B pathways, similar to the three CD20-targeting HexAbs. However, both veltuzumab and rituximab required a higher concentration to be effective and were less efficient in modulating the cell cycle regulators known to promote growth arrest (e.g., up-regulation of p21, p27 and Kip2 and down-regulation of cyclin D1 and phosphorylated Rb). Other notable differences included the inability of veltuzumab or rituximab to alter the levels of phosphorylated p38 and PTEN from untreated controls, whereas all three HexAbs increase phosphorylated p38 and PTEN levels significantly. The decrease in phosphorylated ERKs and the increase in phosphorylated p38 were also observed for the three CD20-targeting HexAbs in Raji cells; (iii) The apoptosis and inhibition of cell proliferation resulting from crosslinking veltuzumab or rituximab with a secondary antibody involves signaling events that were distinguishable from those associated with the CD20-targeting HexAbs, as manifested in phosphorylated ERK (increase vs. decrease), intracellular calcium (increase vs. no change), and mitochondrial membrane potential (loss vs. no change). Intriguingly, these effects translated to notable differences with regard to their relative potency for killing normal human B cells vs. human Burkitt lymphoma cells ex-vivo, because the bispecific 22-(20)-(20) and 20-(22)-(22) showed a higher toxicity to malignant than normal B cells, compared to veltuzumab and rituximab [36]. Thus, the potential advantages of lacking CDC and the moderate but significant enhancement of ADCC

observed for 22-(20)-(20), as compared to epratuzumab, may lead to a more potent anti-lymphoma agent for clinical use.

3.2.2. bsHexAbs that Target CD20 and CD74

During the course of evaluating 22-(20)-(20) and 20-(22)-(22), we noted that neither bsHexAb was capable of inducing direct cytotoxicity in JeKo-1, a mantle cell lymphoma (MCL) line expressing comparable levels of CD22 and CD20 as Daudi cells. On the other hand, 20-(74)-(74) and 74-(20)-(20), the bsHexAbs derived from veltuzumab and milatuzumab, were highly cytotoxic when tested in JeKo-1 and two other MCL lines (Granta-519 and Mino), as well as in primary tumor cells from patients with MCL or CLL, all of which, in the absence of a crosslinking Ab, responded poorly to veltuzumab or milatuzumab alone or combined [38]. Follow-up experiments to interrogate the intracellular events triggered by simultaneously ligating both CD20 and CD74, which could conceivably result only from the binding engagement via either bsHexAb or from crosslinking the 2 parental Abs with a secondary Ab, revealed the prominent roles of actin reorganization and lysosomal membrane permeabilization in the mechanisms of cell death. In addition, the juxtaposition of CD20 and CD74 on MCL cells by the bsHexAbs also induced homotypic adhesion and set off intracellular changes that included loss of mitochondrial transmembrane potential, production of reactive oxygen species, rapid and sustained phosphorylation of ERKs and JNK, and down-regulation of pAkt and Bcl-xL. In an *ex vivo* setting, both 20-(74)-(74) and 74-(20)-(20) displayed a higher potency in depleting lymphoma cells than normal B cells from whole blood [38].

3.3. Pharmacokinetics (PK) and in Vivo Anti-Tumor Activity

We used a bispecific ELISA to quantify the amount of 20-(22)-(22) and 22-(20)-(20) in serum samples collected from PK studies in BALB/c mice and found [36] the two bsHexAbs displayed a shorter circulating half-life than their parental antibodies (24 to 37 h vs. 46 to 52 h). Because both bsHexAbs were stable in serum when assessed *in vitro*, their faster blood clearance was likely due to intracellular breakdown of the modular components, which presumably occurred after their uptake via the FcRn in the vascular endothelium of mice. Evidence for the slow dissociation of the bsHexAbs *in vivo* was provided by SE-HPLC analysis of the PK samples obtained 72 h after injecting radiolabeled 20-(22)-(22), which identified the presence of a new peak with a size of an IgG shown to be derived from veltuzumab, not epratuzumab, since it failed to bind the anti-idiotypic antibody to epratuzumab. A parallel study using radiolabeled 22-(20)-(20) also revealed the presence in the 72-h PK samples of a new peak with a size of an IgG shown to be derived from epratuzumab, not veltuzumab, using an anti-idiotypic antibody to veltuzumab.

The *in vivo* anti-tumor efficacy of 22-(20)-(20) and 20-(22)-(22) was evaluated in SCID mice with a disseminated Daudi model in three studies [36]. In the first study, 22-(20)-(20) and 20-(22)-(22) each were administered i.v. in a single dose of 10 pmol (~3.7 µg) and compared with various controls, including 22-(14)-(14), 20-(14)-(14), 22-(22)-(22), and veltuzumab, giving an equimolar dose. With therapy starting one day after inoculating Daudi cells i.v., the group treated with 22-(20)-(20) had a significantly extended median survival time (MST) compared to the saline control (36 vs. 29 days, $P = 0.005$), whereas the two groups treated with 22-(22)-(22) or 22-(14)-(14) did not improve survival

over saline (29 days, $P = 1.0$). The MST of mice treated with 20-(22)-(22) was significantly longer than the saline control (50 vs. 29 days, $P = 0.005$), but there was no statistically significant difference in the MST of 20-(22)-(22), 20-(14)-(14) and hA20 IgG.

In the second study, we compared the efficacy of 22-(20)-(20) to epratuzumab, 22-(14)-(14), 734-(20)-(20), and a mixture of 22-(14)-(14) and 734-(20)-(20). Groups of 10 mice were administered 10- μ g doses of 22-(20)-(20), 734-(20)-(20), 22-(14)-(14), or 10 μ g of both 734-(20)-(20) and 22-(14)-(14) on days 1, 4 and 7. Additional groups received an equimolar dose of epratuzumab (4 μ g) or saline. All mice in the saline-treated group died within 4 weeks (MST = 25 days). The MSTs for mice treated with 22-(20)-(20), 734-(20)-(20), 22-(14)-(14), the combination, and epratuzumab, were 66.5 days, 42 days, 32 days, 68.5 days, and 32 days, respectively. A statistically significant difference ($P < 0.001$) in the MST was found between 22-(20)-(20) and each of 734-(20)-(20), 22-(14)-(14), and epratuzumab. Notably, the MST of 22-(20)-(20) was about the same as the combination of 734-(20)-(20) and 22-(14)-(14), despite that the latter group providing the same number of CD20- and CD22-binding arms with twice the number of Fc groups.

In the third study, we examined the role of effector cells in the ability of 22-(20)-(20) or 20-(22)-(22) to inhibit tumor growth. Groups of 5 mice depleted of NK cells and neutrophils were administered i.v. with 230 μ g of 22-(20)-(20) or 20-(22)-(22) on days 1, 3, 5, and 9. As controls, four groups of mice without depletion of NK cells and neutrophils were each treated with saline, epratuzumab (100 μ g), or the two bsHexAbs at the same dose and schedule as the depleted groups. Treatments with 22-(20)-(20) or 20-(22)-(22) resulted in no survival benefit compared to animals in the depleted groups, since there was insignificant difference in the MST from the saline control (18 days vs. 21 days). In contrast, treatment of animals in the non-depleted groups with either 22-(20)-(20) or 20-(22)-(22) significantly ($P < 0.002$) increased their survival, with MSTs of 63 and 91 days, respectively, compared to 21 days of the saline control and 28 days of the epratuzumab control. However, the observed difference in the MSTs between the 22-(20)-(20) and 20-(22)-(22) was not statistically significant, perhaps because the relatively small number of animals included in these groups. These initial results underscore the importance of ADCC as the major mechanism of action in retarding tumor growth in animal models by antibodies that target CD20, CD22, or both.

We also evaluated the anti-tumor activity of 20-(74)-(74) and 74-(20)-(20) in SCID mice bearing disseminated JeKo-1 xenografts [38]. Seven groups of 8 mice each were inoculated i.v. with JeKo-1 (2.5×10^7 cells per animal), and after 7 days, each bsHexAb was given in 3 different doses (370, 37, and 3.7 μ g) to a designated group by i.p. injection twice weekly for 2 weeks. Control mice received only saline. Treatment with either bsHexAb at all 3 doses significantly improved survival compared with the saline control animals, which succumbed to disease progression by day 34. Groups treated with the highest dose of 74-(20)-(20) had a 30% increase in MST over saline controls (43.5 days vs. 34 days; $P = 0.0001$). A 60% increase in MST (53 days) over saline controls was observed in the group treated with 20-(74)-(74) at 370 μ g ($P = 0.0001$). Both bsHexAbs given at 370 μ g were more effective than the 2 lower doses ($P = 0.0143$). However, no significant differences were observed between groups treated with 20-(74)-(74) and 74-(20)-(20) at the same dose. These results indicate acceptable stability and dose-dependent antitumor activity of such bsHexAbs *in vivo*.

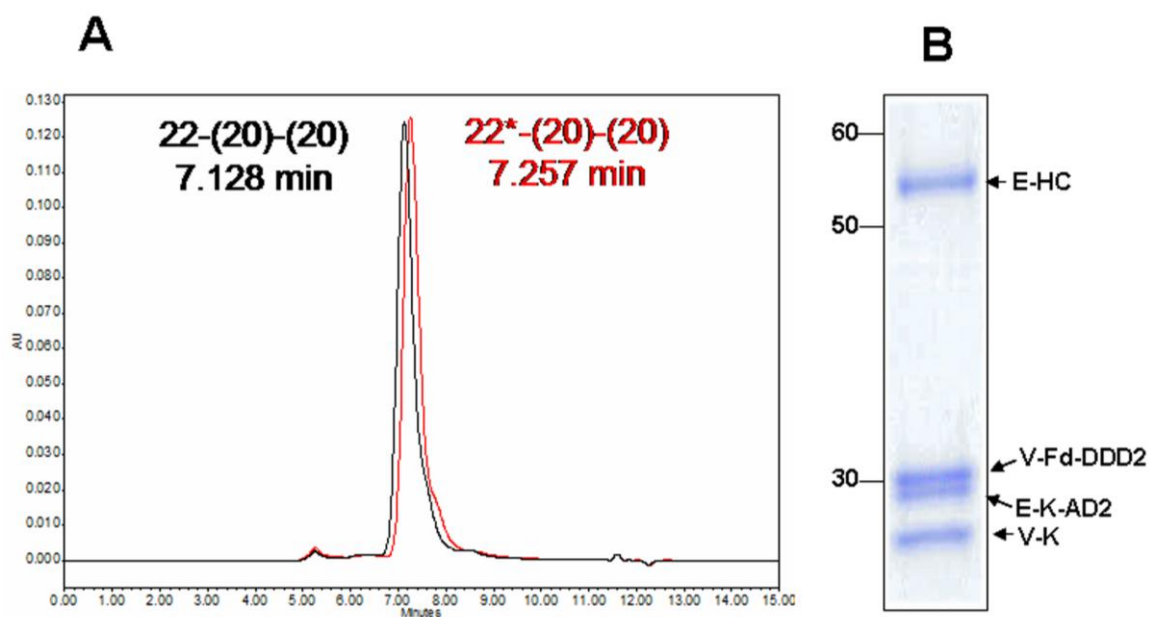
4. The C_K-format of bsHexAbs

The search for increased effector functions as well as a more favorable PK of the C_{H3}-based bsHexAbs led us to explore the potential of their C_K-based counterparts (Figure 2B), in which the AD2 sequence was fused at the C-terminus of the kappa light chain of the intact IgG, resulting in a new series of bsHexAbs denoted as X^{*}-(Y)-(Y), where the C_K-AD2-IgG-X and the dimeric C_{H1}-Fab-DDD2-Y are identified as X^{*} and (Y), respectively. Such notations allow a prompt discern of the C_K-based from the C_{H3}-based HexAbs. For example, 22^{*}-(20)-(20) and 22-(20)-(20) represent two different bsHexAbs, comprising a pair of dimeric C_{H1}-Fab-DDD2-hA20 linked to C_K-AD2-IgG-hLL2 and C_{H3}-IgG-AD2-hLL2, respectively. The results obtained from comparing 22^{*}-(20)-(20) with 22-(20)-(20), as reported recently [40] and highlighted below, indicate the bsHexAbs with the C_K-format not only bind to target cells as efficiently as the C_{H3}-format, but also exhibit superior Fc effector functions *in vitro*, as well as improved PK, stability, and anti-lymphoma activity *in vivo*, thus being favored for future clinical development.

4.1. Generation and *in Vitro* Characterization

C_K-AD2-hLL2-IgG was engineered with the AD2 peptide fused to the C-terminus of the kappa light chain via a hinge linker of 16-amino acid residues (EFPKPSTPPGSSGGAP), expressed in stably-transfected mammalian cells, purified from batch or fed-batch cultures, and reacted with C_{H1}-Fab-DDD2-hA20 to form 22^{*}-(20)-(20), which was similar in molecular size to 22-(20)-(20) by SE-HPLC analysis (Figure 3A), and shown by reducing SDS-PAGE to comprise only the four constitutive polypeptides as designed (Figure 3B).

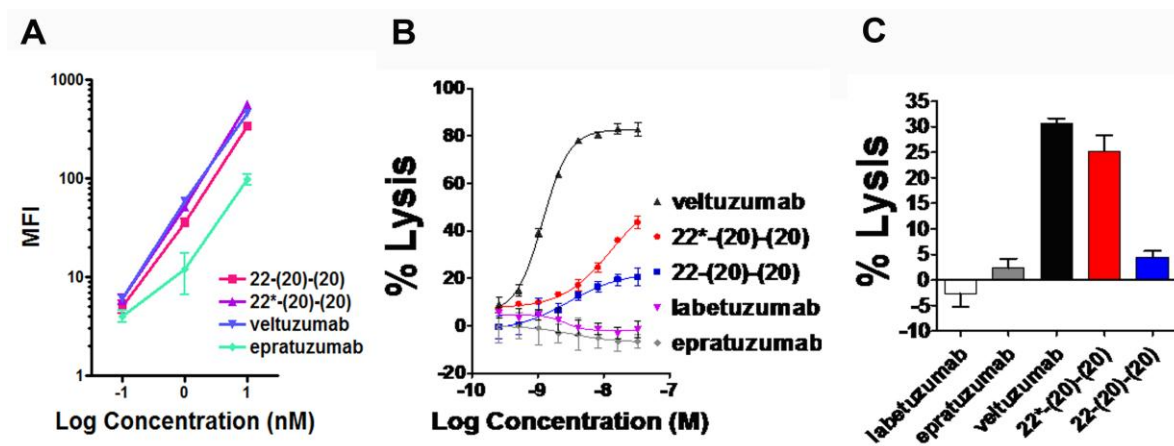
Figure 3. SE-HPLC profile (A) and SDS-PAGE analysis (B) of 22^{*}-(20)-(20). Adapted from Reference [40].



Binding of 22*-(20)-(20) to Daudi cells was compared with that of 22-(20)-(20), epratuzumab and veltuzumab, respectively, using PE-labeled samples [40]. The results shown in Figure 4A indicate 22*-(20)-(20) binds the same as veltuzumab, and appears to display a slightly higher affinity than 22-(20)-(20). Moreover, the equivalency of binding to CD20 on Daudi cells also was demonstrated [40] with 20*-2b and 20-2b, which contain four copies of IFN- α 2b linked to C_K-AD2-hA20-IgG and C_H3-AD2-IgG-hA20, respectively.

Unlike 22-(20)-(20), which was previously noted to display no measureable CDC and only weak ADCC, we found that 22*-(20)-(20) induced moderate CDC (Figure 4B) and exhibited a potent ADCC similar to veltuzumab (Figure 4C). These results implicate a potential strategy for imparting CDC and ADCC to an IgG with little or weak effector functions, such as epratuzumab, by constructing a bsHexAb of the C_K-format in which the IgG of interest is linked to multiple antigen-binding fragments derived from a different antibody with potent effector functions.

Figure 4. Comparison of target cell binding (A), CDC (B) and ADCC (C) of 22*-(20)-(20), 22-(20)-(20) with parental (epratuzumab, veltuzumab) and isotype-control (labetuzumab) antibodies. Adapted from Reference [40].



4.2. Evaluation of PK and in Vivo Anti-Tumor Activity

In both mice and rabbits, the PK parameters determined for 22*-(20)-(20) were similar to those of the parental epratuzumab, but more favorable than those of 22-(20)-(20), achieving about 2-fold higher concentrations in serum, with longer circulating half-life and mean residence time, culminating in 3- to 4-fold greater area under the curve [40]. Consistent with the PK data, the apparent dissociation constants of 22*-(20)-(20) and 22-(20)-(20) for FcRn, as assessed by surface plasmon resonance, were found to be significantly different (166 vs. 310 nM; $P = 0.01$), which may reflect the greater *in vivo* stability of 22*-(20)-(20).

The superiority of 22*-(20)-(20) over 22-(20)-(20) was demonstrated in a disseminated Daudi model, in which animals were administered 22*-(20)-(20) or 22-(20)-(20) in two injections (on days 1 and 5) of high (1 mg) or low (10 μ g) doses [40]. For the high dose, the MST was >130 and 71 days with 100% and 10% survival for 22*-(20)-(20) and 22-(20)-(20), respectively ($P < 0.0001$). With the low-dose treatment, the MST was 91 days for 22*-(20)-(20) with two mice surviving, compared to 50.5 days for 22-(20)-(20) with no survivors ($P = 0.0014$). When given at the high dose, both 22*-(20)-(20)

and 22-(20)-(20) improved survival significantly ($P < 0.0001$) more than the molar equivalent epratuzumab either alone or in combination with C_H1-DDD2-Fab-hA20. Although both bsHexAb given at the low dose also were better than high-dose epratuzumab ($P < 0.003$), only 22*-(20)-(20), not 22-(20)-(20), excelled over the high-dose combination of epratuzumab and C_H1-DDD2-Fab-hA20 ($P < 0.0001$).

5. Conclusions and Future Challenges

Since its inception in 2005, the DNL method, by combining DDD2- and AD2 modules derived from assorted classes of molecules that include antibodies [36,38,58,59], antibody fragments [32,61,62], cytokines [40,52,63,64], polyethylene glycols [57], and enfuvirtide [65], has provided over 100 different complexes with potential applications for targeted therapies of malignant, autoimmune and infectious diseases. As more modules develop, we envision a continuous expansion of the repertoire such that the ultimate promise of multivalent and multispecific agents for treating certain unmet medical needs may be fulfilled with their advantages of more selective and sustained binding to the target cells, potent effector functions, designed capability to inhibit multiple survival pathways, acquired ability to impart novel apoptotic signals, and constitutive cytotoxic activity. For HexAbs in general and bsHexAbs in particular, the future challenges lie in the identification of optimal pairs of parental antibodies for assembly into the C_K-format to deliver effective therapy of solid cancers. We anticipate 22*-(20)-(20) to be the first DNL-based bispecific hexavalent antibody for clinical evaluation in patients with diseases involving abnormal B cells or B-cell malignancies.

In closing, we should note that there are other multimerization approaches to generate bispecific antibodies, among which the “trimerbodies,” as described only recently by Blanco-Toribior and her coworkers [66], were also designed as hexavalent antibodies, whereby its bispecific format is capable of binding to each target antigen trivalently. Such “trimerbodies” lack the Fc domain, can be generated by fusing single-chain variable fragments (scFv) with the same or different specificity to both N- and C-terminus of the trimerizing scaffold domain derived from human collagen XVIII noncollagenous-1 domain, and are produced as soluble proteins in mammalian cells. Beside HexAbs and “trimerbodies,” alternative designs for hexavalent antibodies via recombinant methods, chemical conjugation, or a combination of both, are certainly conceivable. However, a discussion assessing the DNL and other potential approaches is beyond the scope of the current review, whose main purpose is to provide an up-to-date account on the development of bispecific, hexavalent antibodies using the DNL method.

Conflict of Interest

All authors are employees of Immunomedics, which is actively developing novel agents based on the DNL™ platform for treating malignant, autoimmune, and infectious diseases. The authors declare no conflict of interest.

References

1. Reichert, J.M. What are the antibodies to watch in 2013? *mAbs* **2013**, *5*, 1–4.
2. Leonard, J.P.; Coleman, M.; Ketas, J.; Ashe, M.; Fiore, J.M.; Furman, R.R.; Niesvizky, R.; Shore, T.; Chadburn, A.; Horne, H.; *et al.* Combination antibody therapy with epratuzumab and rituximab in relapsed or refractory non-Hodgkin's lymphoma. *J. Clin. Oncol.* **2005**, *23*, 5044–5051.

3. Strauss, S.J.; Morschhauser, F.; Rech, J.; Repp, R.; Solal-Celigny, P.; Zinzani, P.L.; Engert, A.; Coiffier, B.; Hoelzer, D.F.; Wegener, W.A.; *et al.* Multicenter phase II trial of immunotherapy with the humanized anti-CD22 antibody, epratuzumab, in combination with rituximab, in refractory or recurrent non-Hodgkin's lymphoma. *J. Clin. Oncol.* **2006**, *24*, 3880–3886.
4. Leonard, J.P.; Schuster, S.J.; Emmanouilides, C.; Couture, F.; Teoh, N.; Wegener, W.A.; Coleman, M.; Goldenberg, D.M. Durable complete responses from therapy with combined epratuzumab and rituximab: Final results from an international multicenter, phase 2 study in recurrent, indolent, non-Hodgkin lymphoma. *Cancer* **2008**, *113*, 2714–2723.
5. Tonra, J.R.; Corcoran, E.; Deevi, D.S.; Steiner, P.; Kearney, J.; Li, H.; Ludwig, D.L.; Zhu, Z.; Witte, L.; Surguladze, D.; *et al.* Prioritization of EGFR/IGF-IR/VEGFR2 combination targeted therapies utilizing cancer models. *Anticancer Res.* **2009**, *29*, 1999–2008.
6. Alinari, L.; Yu, B.; Christian, B.A.; Yan, F.; Shin, J.; Lapalombella, R.; Hertlein, E.; Lustberg, M.E.; Quinion, C.; Zhang, X.; *et al.* Combination anti-CD74 (milatuzumab) and anti-CD20 (rituximab) monoclonal antibody therapy has *in vitro* and *in vivo* activity in mantle cell lymphoma. *Blood* **2011**, *117*, 4530–4541.
7. Loisel, S.; Andre, P.A.; Golay, J.; Buchegger, F.; Kadouche, J.; Cerutti, M.; Bologna, L.; Kosinski, M.; Viertl, D.; Delaloye, A.B.; *et al.* Antitumour effects of single or combined monoclonal antibodies directed against membrane antigens expressed by human B cells leukaemia. *Mol. Cancer* **2011**, *10*, 42.
8. Skartved, N.J.; Jacobsen, H.J.; Pedersen, M.W.; Jensen, P.F.; Sen, J.W.; Jorgensen, T.K.; Hey, A.; Kragh, M. Preclinical pharmacokinetics and safety of Sym004: A synergistic antibody mixture directed against epidermal growth factor receptor. *Clin. Cancer Res.* **2011**, *17*, 5962–5972.
9. Fuentes, G.; Scaltriti, M.; Baselga, J.; Verma, C.S. Synergy between trastuzumab and pertuzumab for human epidermal growth factor 2 (Her2) from colocalization: An *in silico* based mechanism. *Breast Cancer Res.* **2011**, *13*, R54.
10. Dong, J.; Demarest, S.J.; Sereno, A.; Tamraz, S.; Langley, E.; Doern, A.; Snipas, T.; Perron, K.; Joseph, I.; Glaser, S.M.; *et al.* Combination of two insulin-like growth factor-I receptor inhibitory antibodies targeting distinct epitopes leads to an enhanced antitumor response. *Mol. Cancer Ther.* **2010**, *9*, 2593–2604.
11. Kontermann, R.B. Dual targeting strategies with bispecific antibodies. *mAbs* **2012**, *4*, 182–197.
12. Schubert, I.; Stein, C.; Fey, G.H. Dual-targeting for the elimination of cancer cells with increased selectivity. *Antibodies* **2012**, *1*, 1–18.
13. van der Neut Kolfshoten, M.; Schuurman, J.; Losen, M.; Bleeker, W.K.; Martinez-Martinez, P.; Vermeulen, E.; den Bleker, T.H.; Wiegman, L.; Vink, T.; Aarden, L.A.; *et al.* Anti-inflammatory activity of human IgG4 antibodies by dynamic Fab arm exchange. *Science* **2007**, *317*, 1554–1557.
14. Burton, D.R.; Wilson, I.A. Immunology. Square-dancing antibodies. *Science* **2007**, *317*, 1507–1508.
15. Labrijn, A.F.; Buijsse, A.O.; van den Bremer, E.T.J.; Verwilligen, A.Y.W.; Bleeker, W.K.; Thorpe, S.J.; Killestein, J.; Polman, C.H.; Aalberse, R.C.; Schuurman, J.; *et al.* Therapeutic IgG4 antibodies engage in Fab-arm exchange with endogenous human IgG4 *in vivo*. *Nat. Biotechnol.* **2009**, *27*, 767–771.
16. Milstein, C.; Cuello, A.C. Hybrid hybridomas and their use in immunochemistry. *Nature* **1983**, *305*, 537–540.

17. Staerz, U.D.; Bevan, M.J. Hybrid hybridoma producing a bispecific monoclonal antibody that can focus effector T-cell activity. *Proc. Nat. Acad. Sci. USA* **1986**, *83*, 1453–1457.
18. Perez, P.; Hoffman, R.W.; Shaw, S.; Bluestone, J.A.; Segal, D.M. Specific targeting of cytotoxic T cells by anti-T3 linked to anti-target cell antibody. *Nature* **1985**, *316*, 354–356.
19. Brennan, M.; Davison, P.F.; Paulus, H. Preparation of bispecific antibodies by chemical recombination of monoclonal immunoglobulin G1 fragments. *Science* **1985**, *229*, 81–83.
20. Glennie, M.J.; McBride, H.M.; Worth, A.T.; Stevenson, G.T. Preparation and performance of bispecific F(ab' gamma)2 antibody containing thioether-linked Fab' gamma fragments. *J. Immunol.* **1987**, *139*, 2367–2375.
21. Kriangkum, J.; Xu, B.; Nagata, L.P.; Fulton, R.E.; Suresh, M.R. Bispecific and bifunctional single chain recombinant antibodies. *Biomol. Eng.* **2001**, *18*, 31–40.
22. Muller, D.; Kontermann, R.E. Recombinant bispecific antibodies for cellular cancer immunotherapy. *Curr. Opin. Mol. Ther.* **2007**, *9*, 319–326.
23. Hollander, N. Bispecific antibodies for cancer therapy. *Immunotherapy* **2009**, *1*, 211–222.
24. Marvin, J.S.; Zhu, Z. Recombinant approaches to IgG-like bispecific antibodies. *Acta Pharmacol. Sin.* **2005**, *26*, 649–658.
25. Coloma, M.J.; Morrison, S.L. Design and production of novel tetravalent bispecific antibodies. *Nat. Biotechnol.* **1997**, *15*, 159–163.
26. Lu, D.; Zhang, H.; Ludwig, D.; Persaud, A.; Jimenez, X.; Burtrum, D.; Balderes, P.; Liu, M.; Bohlen, P.; Witte, L.; *et al.* Simultaneous blockade of both the epidermal growth factor receptor and the insulin-like growth factor receptor signaling pathways in cancer cells with a fully human recombinant bispecific antibody. *J. Biol. Chem.* **2004**, *279*, 2856–2865.
27. Lu, D.; Zhang, H.; Koo, H.; Tonra, J.; Balderes, P.; Prewett, M.; Corcoran, E.; Mangalampalli, V.; Bassi, R.; Anselma, D.; *et al.* A fully human recombinant IgG-like bispecific antibody to both the epidermal growth factor receptor and the insulin-like growth factor receptor for enhanced antitumor activity. *J. Biol. Chem.* **2005**, *280*, 19665–19672.
28. Shen, J.; Vil, M.D.; Jimenez, X.; Iacolina, M.; Zhang, H.; Zhu, Z. Single variable domain-IgG fusion. A novel recombinant approach to Fc domain-containing bispecific antibodies. *J. Biol. Chem.* **2006**, *281*, 10706–10714.
29. Shen, J.; Vil, M.D.; Jimenez, X.; Zhang, H.; Iacolina, M.; Mangalampalli, V.; Balderes, P.; Ludwig, D.L.; Zhu, Z. Single variable domain antibody as a versatile building block for the construction of IgG-like bispecific antibodies. *J. Immunol. Methods* **2007**, *318*, 65–74.
30. Asano, R.; Watanabe, Y.; Kawaguchi, H.; Fukuzawa, H.; Nakanishi, T.; Umetzu, M.; Hayashi, H.; Katayose, Y.; Unno, M.; Kudo, T.; *et al.* Highly effective recombinant format of a humanized IgG-like bispecific antibody for cancer immunotherapy with retargeting of lymphocytes to tumor cells. *J. Biol. Chem.* **2007**, *282*, 27659–27665.
31. Wu, C.; Ying, H.; Grinnell, C.; Bryant, S.; Miller, R.; Clabbers, A.; Bose, S.; McCarthy, D.; Zhu, R. R.; Santora, L.; *et al.* Simultaneous targeting of multiple disease mediators by a dual-variable-domain immunoglobulin. *Nat. Biotechnol.* **2007**, *25*, 1290–1297.
32. Rossi, E.A.; Goldenberg, D.M.; Cardillo, T.M.; McBride, W.J.; Sharkey, R.M.; Chang, C.H. Stably tethered multifunctional structures of defined composition made by the dock and lock method for use in cancer targeting. *Proc. Natl. Acad. Sci. USA* **2006**, *103*, 6841–6846.

33. Chang, C.H.; Rossi, E.A.; Goldenberg, D.M. The dock and lock method: A novel platform technology for building multivalent, multifunctional structures of defined composition with retained bioactivity. *Clin. Cancer Res.* **2007**, *13*, 5586s–5591s.
34. Rossi, E.A.; Goldenberg, D.M.; Chang, C.H. Complex and defined biostructures with the dock-and-lock method. *Trends Pharmacol. Sci.* **2012**, *33*, 474–481.
35. Rossi, E.A.; Goldenberg, D.M.; Chang, C.H. The Dock-and-Lock method combines recombinant engineering with site-specific covalent conjugation to generate multifunctional structures. *Bioconjug. Chem.* **2012**, *23*, 309–323.
36. Rossi, E.A.; Goldenberg, D.M.; Cardillo, T.M.; Stein, R.; Chang, C.H. Hexavalent bispecific antibodies represent a new class of anticancer therapeutics: 1. Properties of anti-CD20/CD22 antibodies in lymphoma. *Blood* **2009**, *113*, 6161–6171.
37. Gupta, P.; Goldenberg, D.M.; Rossi, E.A.; Chang, C.H. Multiple signaling pathways induced by hexavalent, monospecific, anti-CD20 and hexavalent, bispecific, anti-CD20/CD22 humanized antibodies correlate with enhanced cytotoxicity to B-cell lymphomas and leukemia. *Blood* **2010**, *116*, 3258–3267.
38. Gupta, P.; Goldenberg, D.M.; Rossi, E.A.; Cardillo, T.M.; Byrd, J.C.; Muthusamy, N.; Furman, R.R.; Chang, C.H. Dual-targeting immunotherapy of lymphoma: Potent cytotoxicity of anti-CD20/CD74 bispecific antibodies in mantle cell and other lymphomas. *Blood* **2012**, *119*, 3767–3778.
39. Chang, C.H.; Rossi, E.A.; Sharkey, R.M.; Goldenberg, D.M. The Dock-and-Lock (DNL) approach to novel bispecific antibodies. In *Bispecific Antibodies*; Kontermann, R.E., Ed.; Springer-Verlag: Berlin/Heidelberg, Germany, 2011; Chapter 12, pp. 199–216.
40. Rossi, E.A.; Chang, C.H.; Cardillo, T.M.; Goldenberg, D.M. Optimization of multivalent bispecific antibodies and immunocytokines with improved *in vivo* properties. *Bioconjug. Chem.* **2013**, *24*, 63–71.
41. Baillie, G.S.; Scott, J.D.; Houslay, M.D. Compartmentalisation of phosphodiesterases and protein kinase A: opposites attract. *FEBS Lett.* **2005**, *579*, 3264–3270.
42. Wong, W.; Scott, J.D. AKAP signaling complexes: Focal points in space and time. *Nat. Rev. Mol. Cell Biol.* **2004**, *5*, 959–970.
43. Newlon, M.G.; Roy, M.; Morikis, D.; Hausken, Z.E.; Coghlan, V.; Scott, J.D.; Jennings, P.A. The molecular basis for protein kinase A anchoring revealed by solution NMR. *Nat. Struct. Biol.* **1999**, *6*, 222–227.
44. Carr, D.W.; Stofko-Hahn, R.E.; Fraser, I.D.; Bishop, S.M.; Acott, T.S.; Brennan, R.G.; Scott, J.D. Interaction of the regulatory subunit (RII) of cAMP-dependent protein kinase with RII-anchoring proteins occurs through an amphipathic helix binding motif. *J. Biol. Chem.* **1991**, *266*, 14188–14192.
45. Colledge, M.; Scott, J.D. AKAPs: From structure to function. *Trends Cell Biol.* **1999**, *9*, 216–222.
46. Newlon, M.G.; Roy, M.; Morikis, D.; Carr, D.W.; Westphal, R.R.; Scott, J.D.; Jennings, P.A. A novel mechanism of PKA anchoring revealed by solution structures of anchoring complexes. *EMBO J.* **2001**, *20*, 1651–1662.
47. Rossi, E.A.; Sharkey, R.M.; McBride, W.; Karacay, H.; Zeng, L.; Hansen, H.J.; Goldenberg, D.M.; Chang, C.H. Development of new multivalent-bispecific agents for pretargeting tumor localization and therapy. *Clin. Cancer Res.* **2003**, *9*, 3886s–3896s.

48. Rossi, E.A.; Chang, C.H.; Losman, M.J.; Sharkey, R.M.; Karacay, H.; McBride, W.; Cardillo, T.M.; Hansen, H.J.; Qu, Z.; Horak, I.D.; *et al.* Pretargeting of carcinoembryonic antigen-expressing cancers with a trivalent bispecific fusion protein produced in myeloma cells. *Clin. Cancer Res.* **2005**, *11*, 7122s–7129s.
49. Sharkey, R.M.; Cardillo, T.M.; Rossi, E.A.; Chang, C.H.; Karacay, H.; McBride, W.J.; Hansen, H.J.; Horak, I.D.; Goldenberg, D.M. Signal amplification in molecular imaging by pretargeting a multivalent, bispecific antibody. *Nat. Med.* **2005**, *11*, 1250–1255.
50. Alto, N.M.; Soderling, S.H.; Hoshi, N.; Langeberg, L.K.; Fayos, R.; Jennings, P.A.; Scott, J.D. Bioinformatic design of A-kinase anchoring protein-in silico: A potent and selective peptide antagonist of type II protein kinase A anchoring. *Proc. Natl. Acad. Sci. USA* **2003**, *100*, 4445–4450.
51. Burns-Hamuro, L.L.; Ma, Y.; Kammerer, S.; Reineke, U.; Self, C.; Cook, C.; Olson, G.L.; Cantor, C.R.; Braun, A.; Taylor, S.S. Designing isoform-specific peptide disruptors of protein kinase A localization. *Proc. Natl. Acad. Sci. USA* **2003**, *100*, 4072–4077.
52. Rossi, E.A.; Goldenberg, D.M.; Cardillo, T.M.; Stein, R.; Chang, C.H. CD20-targeted tetrameric interferon- α , a novel and potent immunocytokine for the therapy of B-cell lymphomas. *Blood* **2009**, *114*, 3864–3871.
53. Binz, H.K.; Pluckthun, A. Engineered proteins as specific binding reagents. *Curr. Opin. Biotechnol.* **2005**, *16*, 459–469.
54. Binz, H.K.; Amstutz, P.; Pluckthun, A. Engineering novel binding proteins from nonimmunoglobulin domains. *Nat. Biotechnol.* **2005**, *23*, 1257–1268.
55. Hey, T.; Fiedler, E.; Rudolph, R.; Fiedler, M. Artificial, non-antibody binding proteins for pharmaceutical and industrial applications. *Trends Biotechnol.* **2005**, *23*, 514–522.
56. Hosse, R.J.; Rothe, A.; Power, B.E. A new generation of protein display scaffold for molecular recognition. *Protein Sci.* **2006**, *15*, 14–27.
57. Chang, C.H.; Rossi, E.A.; Cardillo, T.M.; Nordstrom, D.L.; McBride, W.J.; Goldenberg, D.M. A new method to produce monoPEGylated dimeric cytokines shown with human interferon- α 2b. *Bioconjug. Chem.* **2009**, *20*, 1899–1907.
58. Rossi, E.A.; Goldenberg, D.M.; Cardillo, T.M.; Stein, R.; Wang, Y.; Chang, C.H. Novel designs of multivalent anti-CD20 humanized antibodies as improved lymphoma therapeutics. *Cancer Res.* **2008**, *68*, 8384–8392.
59. Chang, C.H.; Wang, Y.; Trisal, P.; Li, R.; Rossi, D.L.; Nair, A.; Gupta, P.; Losman, M.; Cardillo, T.M.; Rossi, E.A.; *et al.* Evaluation of a novel hexavalent humanized anti-IGF-1R antibody and its bivalent parental IgG in diverse cancer cell lines. *PLoS One* **2012**, *7*, e44235.
60. Stein, R.; Qu, Z.; Chen, S.; Rosario, A.; Shi, V.; Hayes, M.; Horak, I.D.; Hansen, H.J.; Goldenberg, D.M. Characterization of a new humanized anti-CD20 monoclonal antibody, IMMU-106, and Its use in combination with the humanized anti-CD22 antibody, epratuzumab, for the therapy of non-Hodgkin's lymphoma. *Clin. Cancer Res.* **2004**, *10*, 2868–2878.
61. Gold, D.V.; Goldenberg, D.M.; Karacay, H.; Rossi, E.A.; Chang, C.H.; Cardillo, T.M.; McBride, W.J.; Sharkey, R.M. A novel bispecific, trivalent antibody construct for targeting pancreatic carcinoma. *Cancer Res.* **2008**, *68*, 4819–4826.

62. Sharkey, R.M.; van Rij, C.M.; Karacay, H.; Rossi, E.A.; Frielink, C.; Regino, C.; Cardillo, T.M.; McBride, W.J.; Chang, C.H.; *et al.* A new tri-Fab bispecific antibody for pretargeting Trop-2-expressing epithelial cancers. *J. Nucl. Med.* **2012**, *53*, 1625–1632.
63. Rossi, E.A.; Rossi, D.L.; Cardillo, T.M.; Stein, R.; Goldenberg, D.M.; Chang, C.H. Preclinical studies on targeted delivery of multiple interferon-alpha-2b to HLA-DR in diverse hematological cancers. *Blood* **2011**, *118*, 1877–1884.
64. Rossi, E.A.; Rossi, D.L.; Stein, R.; Goldenberg, D.M.; Chang, C.H. A bispecific antibody-IFN α 2b immunocytokine targeting CD20 and HLA-DR is highly toxic to human lymphoma and multiple myeloma cells. *Cancer Res.* **2010**, *70*, 7600–7609.
65. Chang, C.H.; Hinkula, J.; Loo, M.; Falkeborn, T.; Li, R.; Cardillo, T.M.; Rossi, E.A.; Goldenberg, D.M.; Wahren, B. A novel class of anti-HIV agents with multiple copies of enfuvirtide enhances inhibition of viral replication and cellular transmission *in vitro*. *PLoS One* **2012**, *7*, e41235.
66. Blanco-Toribio, A.; Sainz-Pastor, N.; Álvarez-Cienfuegos, A.; Merino, N.; Cuesta, A.M.; Sánchez-Martín, D.; Bonet, J.; Santos-Valle, P.; Sanz, L.; Oliva, B.; *et al.* Generation and characterization of monospecific and bispecific hexavalent trimeric antibodies. *mAbs* **2013**, *5*, 70–79.

© 2013 by the authors; licensee MDPI, Basel, Switzerland. This article is an open access article distributed under the terms and conditions of the Creative Commons Attribution license (<http://creativecommons.org/licenses/by/3.0/>).